Title

The localization of PHRAGMOPLAST ORIENTING KINESIN1 at the division site depends on the microtubule-binding proteins TANGLED1 and AUXIN-INDUCED IN ROOT CULTURES9 in Arabidopsis

Journal

The Plant Cell, 34(11)

ISSN

1040-4651

Authors

Mills, Alison M
Morris, Victoria H
Rasmussen, Carolyn G

Publication Date

2022-10-27

DOI

10.1093/plcell/koac266

Peer reviewed

https://doi.org/10.1093/plcell/koac266 THE PLANT CELL 2022: 34: 4583–4599

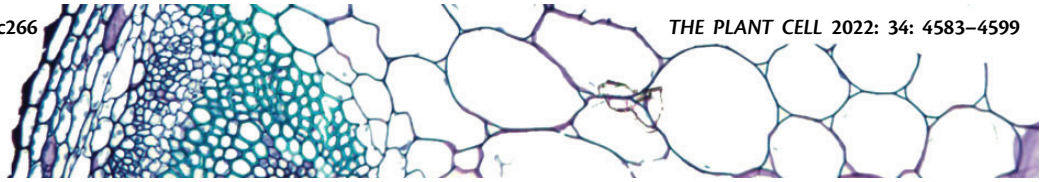

Research Article

The localization of PHRAGMOPLAST ORIENTING KINESIN1 at the division site depends on the microtubule-binding proteins TANGLED1 and AUXIN-INDUCED IN ROOT CULTURES9 in Arabidopsis

Alison M. Mills [1], **Victoria H. Morris** [2,†] **and Carolyn G. Rasmussen** [1,2,*]

1 Graduate Group in Biochemistry and Molecular Biology, University of California, Riverside, California, USA
2 Department of Botany and Plant Sciences, Center for Plant Cell Biology, Institute of Integrative Genome Biology, University of California, Riverside, California, USA

*Author for correspondence: carolyn.rasmussen@ucr.edu
†Present address: Brigham and Women's Hospital, Boston, MA, USA.

A.M.M. and C.G.R. designed the research. A.M.M., V.M., and C.G.R. performed the research. A.M.M., V.M., and C.G.R. contributed new analytic/computational/etc. tools. A.M.M. and C.G.R. analyzed the data, and A.M.M. and C.G.R. wrote the article.
The author responsible for distribution of materials integral to the finding presented in this article in accordance with the policy described in the Instructions for Authors (https://academic.oup.com/plcell) is: Carolyn Rasmussen (carolyn.rasmussen@ucr.edu).

Abstract

Proper plant growth and development require spatial coordination of cell divisions. Two unrelated microtubule-binding proteins, TANGLED1 (TAN1) and AUXIN-INDUCED IN ROOT CULTURES9 (AIR9), are together required for normal growth and division plane orientation in Arabidopsis (*Arabidopsis thaliana*). The *tan1 air9* double mutant has synthetic growth and division plane orientation defects, while single mutants lack obvious defects. Here we show that the division site-localized protein, PHRAGMOPLAST ORIENTING KINESIN1 (POK1), was aberrantly lost from the division site during metaphase and telophase in the *tan1 air9* mutant. Since TAN1 and POK1 interact via the first 132 amino acids of TAN1 ($TAN1_{1-132}$), we assessed the localization and function of $TAN1_{1-132}$ in the *tan1 air9* double mutant. $TAN1_{1-132}$ rescued *tan1 air9* mutant phenotypes and localized to the division site during telophase. However, replacing six amino-acid residues within $TAN1_{1-132}$, which disrupted the POK1–TAN1 interaction in the yeast-two-hybrid system, caused loss of both rescue and division site localization of $TAN1_{1-132}$ in the *tan1 air9* mutant. Full-length TAN1 with the same alanine substitutions had defects in phragmoplast guidance and reduced TAN1 and POK1 localization at the division site but rescued most *tan1 air9* mutant phenotypes. Together, these data suggest that TAN1 and AIR9 are required for POK1 localization, and yet unknown proteins may stabilize TAN1–POK1 interactions.

Introduction

Division plane orientation is important for many aspects of plant, microbial, and animal development, particularly growth and patterning. Division plane orientation is especially relevant for plant cells, which are encased in cell walls and unable to migrate (Facette et al., 2018; Rasmussen and

Received April 26, 2022. Accepted August 08, 2022. Advance access publication August 25, 2022

IN A NUTSHELL

Background: Unlike animal cells, plant cells cannot move due to their semi-rigid cell walls. The correct positioning of the new cell wall is important for overall plant growth and development. Three microtubule-binding proteins are involved in division plane orientation: TANGLED1 (TAN1), AUXIN-INDUCED IN ROOT CULTURES9 (AIR9), and PHRAGMOPLAST ORIENTING KINESIN1 (POK1). These proteins localize as a ring at the edge of the cell where the new cell wall will insert during cell division, at a position called the division site. Here, we focused on how TAN1 and POK1 interactions promote their localization to the division site, and their function in plant growth and division plane positioning.

Question: How do TAN1 and AIR9 contribute to POK1 localization, and how does POK1 localization affect new cell wall placement?

Findings: TAN1 and AIR9 together maintain POK1 at the division site in *Arabidopsis thaliana*. When mutant versions of TAN1 that no longer interact with POK1 were transformed into the *tan1 air9* double mutant, POK1 and TAN1 localization was partially disrupted and cell wall placement defects occurred. This suggests that POK1 interaction with TAN1 is important for their correct division site localization and new cell wall placement.

Next steps: This work strongly suggests that yet unknown proteins mediate TAN1 and POK1 interaction. Discovering what those proteins are, and how AIR9 contributes to division plane positioning are next. Understanding how plants position their division plane will contribute to understanding plant growth and has the long-term potential to contribute to next-generation crop development.

Bellinger, 2018; Wu et al., 2018; Livanos and Müller, 2019). Positioning and construction of a new cell wall (cell plate) during cytokinesis involves two microtubule- and microfilament-rich cytoskeletal structures: the preprophase band (PPB) and the phragmoplast, respectively (Smertenko et al., 2017). The PPB is a ring of microtubules, microfilaments, and proteins that forms at the cell cortex just beneath the plasma membrane during G2; this region is defined as the cortical division zone (Van Damme, 2009; Li et al., 2015; Smertenko et al., 2017). The cortical division zone is characterized by active endocytosis mediated by TPLATE-clathrin-coated vesicles that may deplete actin and the actin-binding kinesin-like protein KCA1/KAC1 (Hoshino et al., 2003; Vanstraelen et al., 2004; Panteris, 2008; Karahara et al., 2009; Suetsugu et al., 2010; Kojo et al., 2013). After nuclear envelope breakdown, the PPB disassembles and the metaphase spindle, an antiparallel microtubule array with its plus-ends directed toward the middle of the cell, forms (Dixit and Cyr, 2002). After the chromosomes are separated, the phragmoplast is constructed from spindle remnants to form another antiparallel array of microtubules (Lee and Liu, 2019). The phragmoplast microtubules are tracks for the movement of vesicles containing cell wall materials toward the forming cell plate (McMichael and Bednarek, 2013; Müller and Jürgens, 2016). The phragmoplast expands by nucleation of new microtubules on preexisting microtubules (Murata et al., 2013; Smertenko et al., 2018) and is partially dependent on the mitotic microtubule-binding protein ENDOSPERM DEFECTIVE1 and the augmin complex to recruit gamma tubulin to phragmoplast microtubules (Nakaoka et al., 2012; Lee et al., 2017). Finally, the phragmoplast reaches the cell cortex, and the cell plate and associated membranes fuse with the mother cell membranes at the cell plate fusion site previously specified by the PPB (van Oostende-Triplet et al., 2017).

TANGLED1 (TAN1, AT3G05330) was the first protein identified to localize to the plant division site throughout mitosis and cytokinesis (Walker et al., 2007). In maize (*Zea mays*), the *tan1* mutant has defects in division plane orientation caused by phragmoplast guidance defects (Cleary and Smith, 1998; Martinez et al., 2017). TAN1 bundles and cross-links microtubules in vitro (Martinez et al., 2020). In vivo, TAN1 promotes microtubule pausing at the division site (Bellinger et al., 2021). TAN1, together with other division site-localized proteins, is critical for the organization of an array of cell cortex-localized microtubules that are independent from the phragmoplast. These cortical-telophase microtubules accumulate at the cell cortex during telophase and are subsequently incorporated into the phragmoplast to direct its movement toward the division site (Bellinger et al., 2021).

Other important division site-localized proteins were identified through their interaction with TAN1, such as the division site-localized kinesin-12 proteins PHRAGMOPLAST ORIENTING KINESIN (POK1) and POK2 (Müller et al., 2006; Lipka et al., 2014). Similar to PHRAGMOPLAST-ASSOCIATED KINESIN-RELATED PROTEIN (PAKRP1) and PAKRPL1 (Pan et al., 2004; Lee et al., 2007), which are other kinesin-12 proteins, POK2 localizes to the phragmoplast midline during telophase and plays a unique role in phragmoplast expansion (Herrmann et al., 2018). Together, POK1 and POK2 are required to guide the phragmoplast to the division site (Müller et al., 2006; Herrmann et al., 2018). The *pok1 pok2* double mutant of Arabidopsis (*Arabidopsis thaliana*) has stunted growth and misplaced cell walls as a result of phragmoplast guidance defects (Müller et al., 2006). The *pok1 pok2* double

mutant also fails to maintain TAN1 at the division site after entry into metaphase (Lipka et al., 2014). This suggests that TAN1 maintenance at the division site after metaphase is dependent on POK1 and POK2.

In Arabidopsis, the *tan1* mutant has minor phenotypic differences compared with wild-type (WT) plants (Walker et al., 2007). However, the *tan1 auxin-induced-in-root-cultures9* (*air9*) double mutant, which has no obvious defects (Buschmann et al., 2015), resulted in a synthetic phenotype consisting of reduced root growth, increased root cell file rotation, and phragmoplast guidance defects (Mir et al., 2018). TAN1 and AIR9 are unrelated microtubule-binding proteins that both localize to the division site (Buschmann et al., 2006; Walker et al., 2007). Both TAN1 and AIR9 colocalize with the PPB. TAN1 remains at the division site throughout cell division, while AIR9 is lost from the division site upon PPB disassembly and then reappears at the division site during cytokinesis when the phragmoplast contacts the cortex. When full-length *TAN1* fused to *YELLOW FLUORESCENT PROTEIN* (*TAN1-YFP*) and driven either by the constitutive viral cauliflower mosaic CaMV35S promoter (p35S:*TAN1-YFP*) or the native promoter with the fluorescent protein as either an N- or C-terminal fusion (pTAN1:*TAN1–YFP* or pTAN1:*CFP–TAN1*) was transformed into the *tan1 air9* double mutant, the phenotype was rescued such that plants looked similar to and grew as well as WT plants (Mir et al., 2018; Mills and Rasmussen, 2022).

TAN1 is an intrinsically disordered protein with no well-defined domains. It was divided into five conserved regions based on alignments of amino acid similarity across plant species. Region I, which covers the first approximately 130 amino acids of TAN1, is the most highly conserved and mediates TAN1 localization to the division site during telophase. This approximately 130 amino acid region also mediates interactions between TAN1 and POK1 in the yeast two-hybrid system (Rasmussen et al., 2011). When *TAN1* missing the sequence for the first approximately 130 amino acids was transformed into the *tan1 air9* double mutant, no rescue was observed (Mir et al., 2018). This suggests that the first approximately 130 amino acids of the TAN1 protein are critical for function in root growth and division plane positioning.

Here, we show that both AIR9 and TAN1 are required for POK1 to remain at the division site after PPB disassembly. We identified TAN1–POK1 interaction motifs within the first 132 amino acids using the yeast two-hybrid system. Interestingly, the first 132 amino acids of TAN1 ($TAN1_{1-132}$) are sufficient to rescue the *tan1 air9* double mutant, but not when a TAN1–POK1 interaction motif was disrupted. We found that when full-length TAN1 with the same mutated motif was used, substantial rescue was observed, except for defects in phragmoplast guidance and loss of POK1 and TAN1 at the division site during metaphase and telophase. Together, this suggests that interactions between POK1 and AIR9, and TAN1 and POK1, as well as other yet unknown proteins, are important for division plane orientation and plant growth.

Results

Either TAN1 or AIR9 is sufficient to recruit and maintain POK1 at the division site

To understand how known division site-localized proteins interact at the division site, we examined POK1 fused to YFP–POK1 (Lipka et al., 2014) localization in WT, *tan1 air9* double mutant and single mutant Arabidopsis plants expressing the microtubule marker *UBQ10:mScarlet-MAP4* (Pan et al., 2020). Our hypothesis was that POK1 localization would not be contingent on TAN1 or AIR9 and would therefore be unaltered in the *tan1 air9* double mutant. In contrast to our hypothesis, YFP–POK1 was lost from the division site during metaphase and telophase and accumulated less frequently during preprophase and prophase. In WT cells, YFP–POK1 colocalized with PPBs in 71% of preprophase/prophase cells (n = 50/70 cells, 15 plants, Figure 1A) consistent with previous observations (Lipka et al., 2014; Schaefer et al., 2017). In the *tan1 air9* double mutant cells, YFP–POK1 colocalized with 50% of PPBs during preprophase/prophase, which was not significantly different from the colocalization rate in WT cells (n = 27/54 cells, 15 plants, Figure 1, D and M; Fisher's exact test, P = 0.0165, not significant with Bonferroni correction). In WT cells, YFP–POK1 remained at the division site in all observed metaphase (n = 13/13 cells, Figure 1B) and telophase cells (n = 31/31 cells, Figure 1C), similar to previous studies (Lipka et al., 2014). In rare instances, YFP–POK1 also accumulated in the phragmoplast midline in WT cells (13%, n = 4/31, 11 plants, Figure 1M). In contrast, in *tan1 air9* mutants, YFP–POK1 was lost from the division site in metaphase (n = 0/21 cells, Figure 1, E and M) and telophase (n = 0/44, Figure 1F). Interestingly, in *tan1 air9* double mutant cells, although YFP–POK1 did not accumulate at the division site, it accumulated at the phragmoplast midline in 77% of cells (n = 34/44), which was a significantly greater midline accumulation frequency than the 13% observed in WT plants (n = 4/31 cells, Fisher's exact test, $P < 0.00001$). Together, this shows that POK1 is not maintained at the division site after PPB disassembly and that instead it accumulates in the phragmoplast midline. We hypothesize that mislocalized phragmoplast midline accumulation of YFP–POK1 in the *tan1 air9* mutant occurs because YFP–POK1 is not maintained at the division site.

Next, we examined YFP–POK1 localization in *tan1* and *air9* single mutants. YFP–POK1 localized to the division site during all mitotic stages, but aberrantly accumulated in the phragmoplast midline in the *tan1* single mutant. Similar to in WT plants, YFP–POK1 colocalized with PPBs during preprophase or prophase in the *tan1* mutant (Figure 1G) and *air9* mutant (Figure 1H), and remained at the division site during metaphase and telophase (Figure 1, G–L and M). In the *tan1* single mutant, YFP–POK1 localized both to the division site and the phragmoplast midline in 44% of

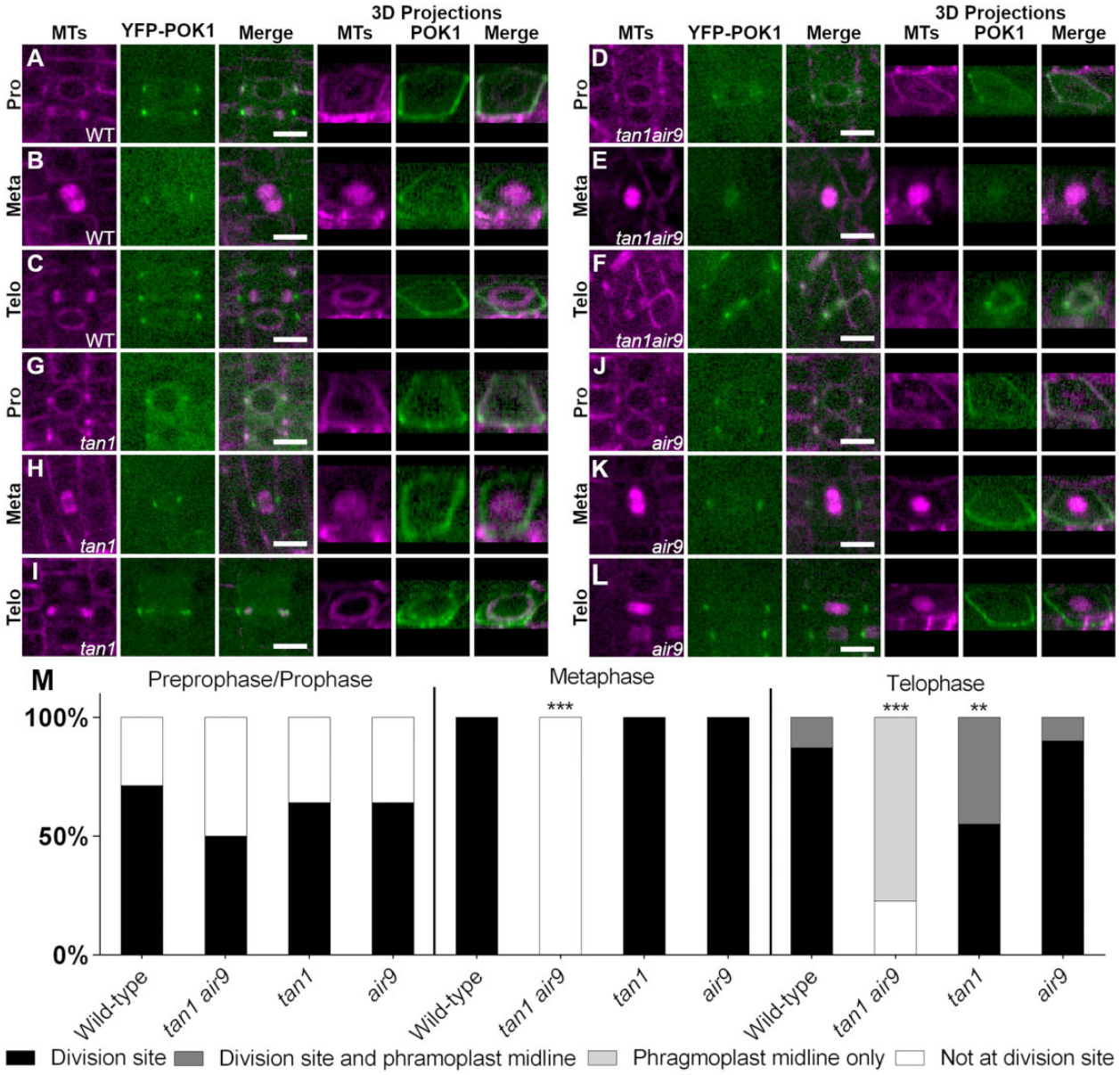

Figure 1 TAN1 and AIR9 together promote POK1 maintenance at the division site. YFP–POK1 localization in Col-0 WT, *tan1* single mutant, *air9* single mutant, and *tan1 air9* double mutant plants expressing UBQ10:mScarlet-*MAP4* to mark microtubules and pPOK1:*YFP–POK1*. Scale bars = 10 μm. A–C, YFP–POK1 localization in Col-0 WT plants. A, YFP–POK1 localization during preprophase/prophase. B, YFP–POK1 was maintained at the division site in metaphase and anaphase cells in Col-0 plants. C, YFP–POK1 remains clearly visible at the division site in Col-0 telophase cells. D–F, YFP–POK1 localization in *tan1 air9* double mutant plants. D, YFP–POK1 localization during preprophase/prophase. E, YFP–POK1 was lost from the division site upon entry into metaphase. F, In *tan1 air9* telophase cells YFP–POK1 was absent from the division site and accumulated in the phragmoplast midline. G–I, YFP–POK1 localization in *tan1* single mutant plants. G, YFP–POK1 localization in the *tan1* single mutant during preprophase/prophase. H, YFP–POK1 was maintained at the division site in metaphase and anaphase cells in *tan1* plants. I, YFP–POK1 remains clearly visible at the division site in *tan1* telophase cells. J–L, YFP–POK1 localization in *air9* single mutant plants. J, YFP–POK1 localization during preprophase/prophase. K, YFP–POK1 was maintained at the division site in metaphase and anaphase cells in *air9* plants. L, YFP–POK1 remains clearly visible at the division site in *air9* telophase. M, YFP–POK1 subcellular localization in WT, *tan1 air9*, *tan1*, and *air9* plants in preprophase/prophase, metaphase, and telophase cells. $N > 14$ plants for each genotype. Statistically significant differences in localization compared to WT plants were determined using Fisher's exact test with Bonferroni correction for four sample types. Asterisks indicate significant differences. YFP–POK1 colocalized with the PPB in 71% of WT cells (50/70), 50% of *tan1 air9* cells (27/54), 64% of *tan1* cells (54/85), and 64% of *air9* cells (46/72). YFP–POK1 colocalization with the PPB was not significantly different in *tan1 air9*, *tan1*, and *air9* plants compared to in Wt plants. YFP–POK1 was maintained at the division site in all metaphase cells of WT (13/13 cells), *tan1* (17/17 cells), and *air9* (24/24 cells) plants. In *tan1 air9* double mutant plants, YFP–POK1 was not maintained at the division site during metaphase (0/21 cells, $P < 0.00001$). During telophase, YFP–POK1 accumulated at the division site only in 87% of WT cells (27/31). In 13% of WT telophase cells, YFP–POK1 accumulated at the division site and in the phragmoplast midline (4/31 cells). YFP–POK1 localization in telophase cells of *air9* single mutant plants was not significantly different from that in WT plants, with 90% of cells (36/40) accumulating YFP–POK1 at the division site only and 10% (4/40) accumulating YFP–POK1

(continued)

telophase cells (Figure 1I, $n = 12/27$), which is a significantly greater midline accumulation rate compared to that in WT plants (13%, $n = 4/31$, 10 plants, Fisher's exact test, $P = 0.0094$) or the *air9* single mutant (Figure 1L, 10%, $n = 4/40$). Aberrant phragmoplast midline accumulation of YFP–POK1 in the *tan1* single mutant suggested that the POK1–TAN1 interaction might be required to maintain POK1 at the division site. This prompted us to examine their interaction more closely.

Amino acids 1–132 of TAN1 rescue the *tan1 air9* double mutant

POK1 interacts with both full-length TAN1 and the first 132 amino acids of TAN1 using the yeast two-hybrid system (Rasmussen et al., 2011). TAN1 missing the first 126 amino acids failed to rescue the *tan1 air9* double mutant, suggesting that this part of the protein is critical for TAN1 function (Mir et al., 2018). To test the function of this region of the protein in Arabidopsis, the *TAN1* coding sequence for the first 132 amino acids was fused to *YFP* (*TAN1*$_{1-132}$*-YFP*) driven by the cauliflower mosaic p35S promoter and was then transformed into the *tan1 air9* double mutant. We used p35S*:TAN1-YFP* in the *tan1 air9* double mutant as our benchmark for rescue, as its ability to rescue the *tan1 air9* double mutant was demonstrated previously (Mir et al., 2018). The progeny of several independent p35S*:TAN1*$_{1-132}$*-YFP* lines rescued the *tan1 air9* double mutant, as described in more detail below. Overall root patterning of *tan1 air9* double mutants expressing either p35S*:TAN1*$_{1-132}$*-YFP* or full-length p35S*:TAN1-YFP* was restored, while untransformed *tan1 air9* double mutant roots had misoriented divisions (Figure 2A; Supplemental Figure S1). Cell file rotation, which skews left and has large variance in the *tan1 air9* double mutant (Figure 2, B and C), was significantly rescued in both p35S*:TAN1*$_{1-132}$*-YFP* and p35S*:TAN1-YFP tan1 air9* lines ($n = 37$ and 41 plants, respectively), compared to the untransformed *tan1 air9* control (Levene's test used due to nonnormal distribution, $P < 0.0001$). Root length at 8 days after stratification was also restored (Figure 2D). Interestingly, although TAN1$_{1-132}$-YFP rarely co-localizes with PPBs in WT plants (Rasmussen et al., 2011) or in the *tan1 air9* double mutant (10%, $n = 9/89$ cells, Figure 3A), PPB angles of p35S*:TAN1*$_{1-132}$*-YFP* and p35S*:TAN1-YFP tan1 air9* plants had significantly less variance compared to the untransformed control (Figure 2E). Phragmoplast positioning defects of the *tan1 air9* double mutant were also significantly rescued by p35S*:TAN1*$_{1-132}$*-YFP*. Altogether, p35S*:TAN1*$_{1-132}$*-YFP* rescued the phenotypes of the double mutant similar to full-length p35S*:TAN1-YFP*. This indicates that most functions that affect phenotypes assessed here are encoded by the first section of the *TAN1* gene.

Disrupting TAN1–POK1 interaction alters TAN1 and POK1 localization to the division site and reduces *tan1 air9* rescue

To further understand how TAN1 functions, we disrupted its ability to interact with the kinesin POK1 using alanine scanning mutagenesis. Alanine scanning mutagenesis was used to replace six amino acids with six alanines across the first approximately 120 amino acids of TAN1$_{1-132}$ (described in the "Materials and methods"). After testing their interaction with POK1 using the yeast two-hybrid system, we identified seven constructs that lost interaction with POK1 (Supplemental Figure S2). Reasoning that highly conserved amino acids would be more likely to play critical roles in the TAN1–POK1 interaction, we selected TAN1$_{1-132}$ with alanine substitutions, replacing the highly conserved amino acids at positions 28–33 (INKVDK) with six alanines (TAN1(28–33A)$_{1-132}$) for analysis in Arabidopsis. Our hypothesis was that the mutated form of TAN1$_{1-132}$ (TAN1(28–33A)$_{1-132}$) would not rescue the *tan1 air9* mutant due to lack of POK1 and TAN1 interaction. *TAN1(28–33A)*$_{1-132}$ was cloned into a plant transformation vector to generate p35S*:TAN1(28–33A)*$_{1-132}$*-YFP* and transformed into the *tan1 air9* double mutant. The p35S*:TAN1(28–33A)*$_{1-132}$*-YFP* construct partially rescued the *tan1 air9* double mutant (Figure 4; Supplemental Figure S3). p35S*:TAN1(28–33A)*$_{1-132}$*-YFP* in the *tan1 air9* double mutant did not rescue cell file rotation defects (Figure 4, B and D) or phragmoplast angle defects (Figure 4F). However, overall plant growth (Figure 4C) and root length (Figure 4E) showed intermediate rescue compared to unaltered p35S*:TAN1*$_{1-132}$*-YFP* in the *tan1 air9* double mutant. PPB angles in *tan1 air9* double mutants expressing either p35S*:TAN1(28–33A)*$_{1-132}$*-YFP* or p35S*:TAN1*$_{1-132}$*-YFP* were similar, suggesting that the TAN1–POK1 interaction may not be required for PPB placement (Figure 4F). These results suggest that the first 132 amino acids of TAN1 perform several vital functions, some of which are contingent or partially contingent on a likely interaction with POK1 in Arabidopsis.

To understand how this mutation within TAN1$_{1\text{-}132}$ affected localization, we analyzed TAN1(28–33A)$_{1-132}$-YFP in the *tan1 air9* double mutant. Localization of TAN1 (28–33A)$_{1-132}$-YFP to the division site in the *tan1 air9* double mutant was significantly reduced compared to that of unaltered TAN1$_{1-132}$-YFP, which localized to the division site during telophase 100% of the time ($n = 58/58$ cells, 29 plants, Figure 3E; Rasmussen et al., 2011). TAN1(28–33A)$_{1-132}$-YFP showed no obvious division site localization 68% of the

Figure 1 (Continued)
at the division site and in the phragmoplast midline. In *tan1* single mutant plants, YFP–POK1 was present at the division site in all telophase cells but accumulated more frequently at the division site and phragmoplast midline compared to in WT plants (44%; 12/27 cells; $P = 0.0094$). In *tan1 air9* double mutant plants, YFP–POK1 never accumulated at the division site of telophase cells and instead accumulated solely in the phragmoplast midline (34/44 cells, $P < 0.00001$).

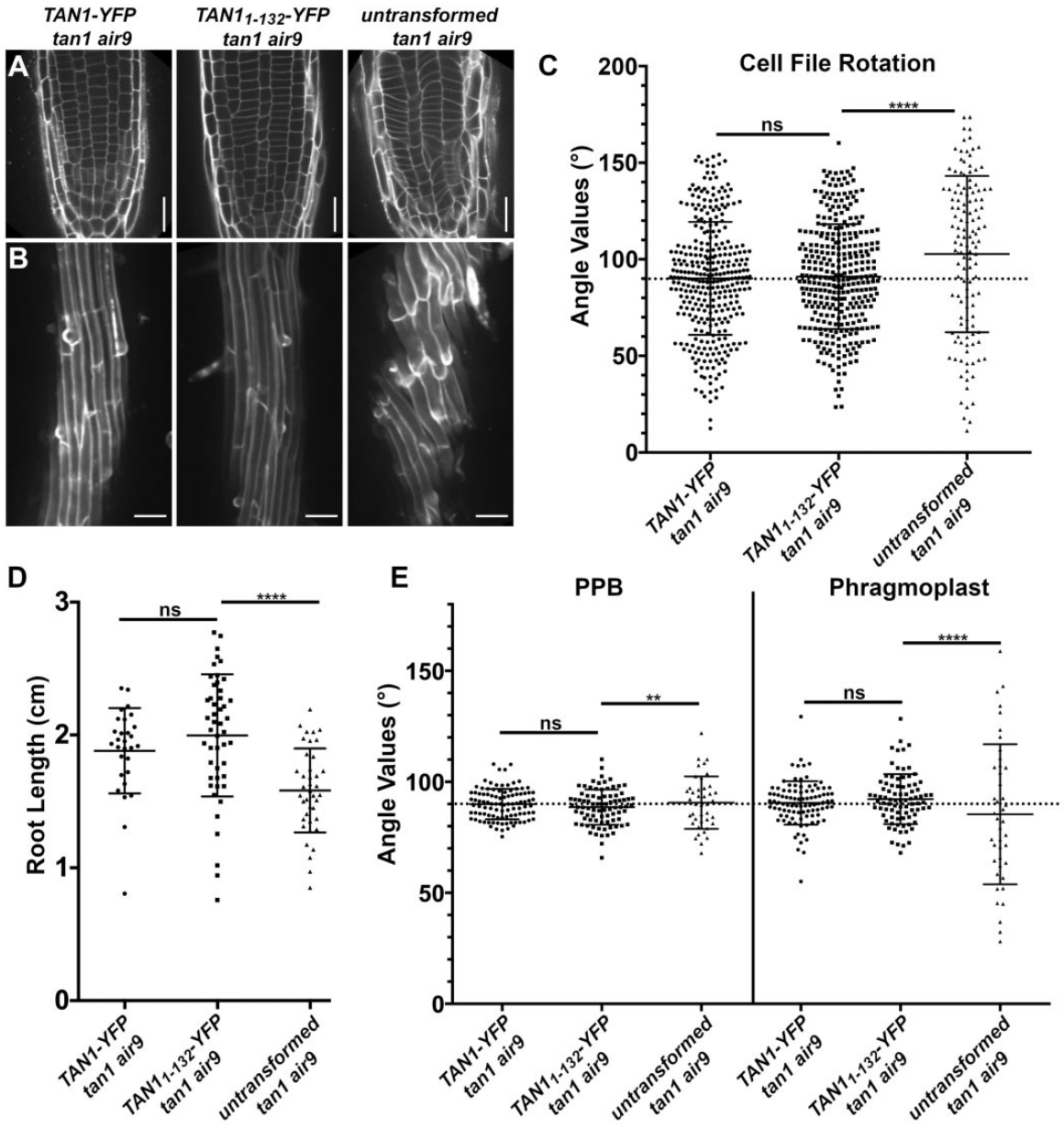

Figure 2 p35S:*TAN1*$_{1-132}$-*YFP* rescues Arabidopsis *tan1 air9* double mutant phenotypes. A, Cell walls stained with PI of *tan1 air9* double mutant root tips expressing p35S:*TAN1-YFP* (left) and p35S:*TAN1*$_{1-132}$-*YFP* (middle), and untransformed *tan1 air9* double mutant root tips (right). Bars = 25 μm. B, Maximum projections of 10 1-μm Z-stacks of PI-stained differentiation zone root cell walls. Scale bars = 50 μm. C, Cell file rotation angles of *tan1 air9* double mutants expressing p35S:*TAN1-YFP* (left), p35S:*TAN1*$_{1-132}$-*YFP* (middle), and untransformed plants (right), $n > 13$ plants for each genotype. Each dot represents an angle measured from the left side of the long axis of the root to the transverse cell wall. Angle variances were compared with Levene's test due to nonnormal distribution. D, Root length measurements from 8 days after stratification of *tan1 air9* double mutants expressing p35S:*TAN1-YFP* (left), p35S:*TAN1*$_{1-132}$-*YFP* (middle), and untransformed plants (right), $n > 28$ plants for each genotype, compared by two-tailed *t* test with Welch's correction. E, PPB and phragmoplast angle measurements in *tan1 air9* double mutant cells expressing p35S:*TAN1-YFP* (left), p35S:*TAN1*$_{1-132}$-*YFP* (middle), and untransformed plants (right), $n > 20$ plants for each genotype. Angle variations compared with *F*-test. C–E, Mean and standard deviation are indicated. ns indicates not significant, $^{**}P < 0.01$, $^{****}P < 0.0001$

time (n = 15/22 cells, Figure 3I) or faint division site accumulation in 32% of telophase cells (n = 7/22 cells, Figure 3J). When the fluorescence intensity of TAN1(28–33A)$_{1-132}$-YFP at the division site during telophase was compared to the cytosolic fluorescence intensity in the same cell, the median ratio was ∼1.1, indicating little preferential accumulation of TAN1(28–33A)$_{1-132}$-YFP at the division site (Figure 3K). In contrast, the median ratio of unaltered TAN1$_{1-132}$-YFP at the division site was ∼1.8 compared to cytosolic fluorescence, indicating its preferential accumulation at the division site. This suggests that TAN1 requires the motif in amino acids 28–33 to localize properly to the division site during telophase. Our hypothesis is that this reduced localization is due to disruptions in the TAN1$_{1-132}$–POK1 interaction.

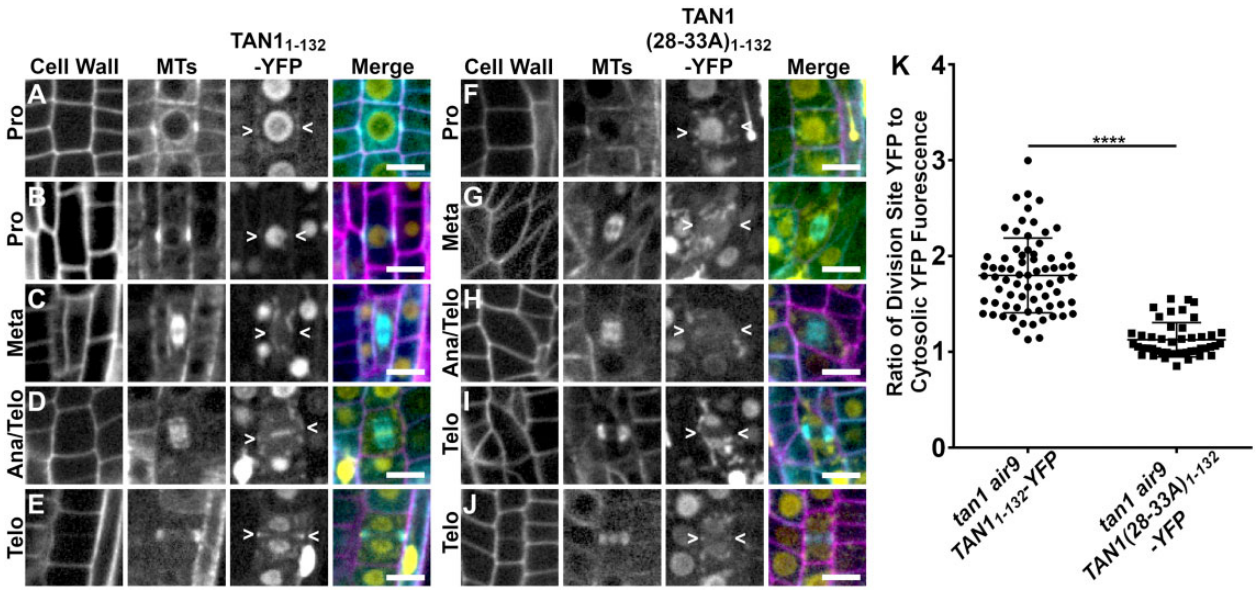

Figure 3 Division site localization during telophase is common for TAN1$_{1-132}$-YFP but rare for TAN1(28–33A)$_{1-132}$-YFP in *tan1 air9* double mutant cells. A–E, PI-stained *tan1 air9* plants expressing p35S:*TAN1$_{1-132}$-YFP and CFP-TUBULIN* during mitosis (n = 29 plants). The division site is indicated by arrowheads in the YFP panels. Scale bars = 10 µm. A, Rare prophase division site accumulation of TAN1$_{1-132}$-YFP (10%, n = 9/89 cells), (B) common prophase TAN1$_{1-132}$-YFP nuclear accumulation without division site localization (90%, n = 80/89 cells), (C) no specific TAN1$_{1-132}$-YFP division site accumulation in metaphase (100%, n = 28/28 cells), (D) faint TAN1$_{1-132}$-YFP division site accumulation accompanied by midline accumulation in late anaphase/early telophase (80%, n = 16/20 cells), and (E) TAN1$_{1-132}$-YFP division site accumulation during telophase (100%, n = 58/58 cells). F–H, *tan1 air9* plants expressing p35S:*TAN1(28–33A)$_{1-132}$-YFP* during mitosis (n = 13 plants). The division site is indicated by arrowheads in the YFP panels. F, No specific TAN1(28–33A)$_{1-132}$-YFP prophase division site accumulation during prophase (100%, n = 20/20 cells), (G) no specific TAN1(28–33A)$_{1-132}$-YFP division site accumulation during metaphase (100%, n = 12/12 cells), (H) no TAN1(28–33A)$_{1-132}$-YFP division site or midline accumulation in late anaphase/early telophase (100%, n = 8/8 cells), (I) no specific TAN1(28–33A)$_{1-132}$-YFP division site accumulation during telophase (68%, n = 15/22 cells) and (J) faint TAN1(28–33A)$_{1-132}$-YFP division site accumulation during telophase (32%, n = 7/22 cells). K, Ratio of TAN1$_{1-132}$-YFP (left) or TAN1(28–33A)$_{1-132}$-YFP (right) fluorescence at the division site to cytosolic fluorescence from *tan1 air9* plants expressing p35S:*TAN1$_{1-132}$-YFP* or p35S:*TAN1(28–33A)$_{1-132}$-YFP* during telophase, $n > 23$ plants for each genotype. Mean and standard deviation are indicated. Asterisks indicate a significant difference as determined by Mann–Whitney U test, $P < 0.0001$.

Next, we generated a construct that introduced alanines at amino acids 28–33 in full-length YFP–TAN1 constructs (p35S:*YFP–TAN1(28–33A)*) to assess whether p35S:*YFP–TAN1(28–33A)* would rescue the *tan1 air9* double mutant. In contrast to the modest partial rescue provided by p35S:*TAN1(28–33A)$_{1-132}$-YFP*, full-length p35S:*YFP–TAN1(28–33A)* significantly rescued the defects in the *tan1 air9* double mutant, as described below. First, we assessed whether full-length TAN1(28–33A) interacted with POK1 via the yeast two-hybrid system, and it did not (Supplemental Figure S4). Next, we analyzed rescue in Arabidopsis expressing p35S:*YFP–TAN1(28–33A)*. Most defects, except phragmoplast angle variance (Figure 5; Supplemental Figure S5), were fully rescued in the p35S:*YFP–TAN1(28–33A) tan1 air9* line, including cell file rotation (Figure 5C), root length (Figure 5D), and PPB angles (Figure 5E). Similar to TAN1–YFP, YFP–TAN1(28–33A) localized to the division site in preprophase, prophase, and telophase (Supplemental Figure S6).

To determine if full-length YFP–TAN1(28–33A) had reduced accumulation at the division site during telophase similar to TAN1(28–33A)$_{1-132}$-YFP, fluorescence intensity levels were measured. During prophase, the YFP–TAN1(28–33A) fluorescence intensity at the division site compared to in the cytosol was comparable to the TAN1-YFP fluorescence intensity ratios. In contrast, the YFP–TAN1(28–33A) fluorescence intensity ratios during telophase were reduced to ∼1.6 compared with unaltered TAN1-YFP (∼2.1) indicating that YFP–TAN1(28–33A) accumulated less at the division site during telophase (Supplemental Figure S6). Together, these data suggest that TAN1 is recruited to the division site during prophase without an interaction with POK1. Defects in phragmoplast positioning may be due specifically to the disruption of the TAN1–POK1 interaction in the *tan1 air9* double mutant. Since AIR9 is missing, TAN1 and POK1 interactions may be more important. Moreover, phragmoplast guidance defects may be due to the lower accumulation of TAN1 at the division site that would normally be mediated by POK1 during telophase.

To better understand how these alanine substitutions affect both POK1 and TAN1 localization, we examined *tan1 air9* double mutant plants expressing a microtubule marker (*UBQ10:mScarlet-MAP4*; Pan et al., 2020), pTAN1:*CFP–TAN1(28–33A)* and pPOK1:*YFP–POK1* (Lipka et al., 2014). Both CFP–TAN1(28–33A) and YFP–POK1 had reduced accumulation at the division site in the *tan1 air9* double mutant. CFP–TAN1(28–33A) and YFP–POK1 colocalized with

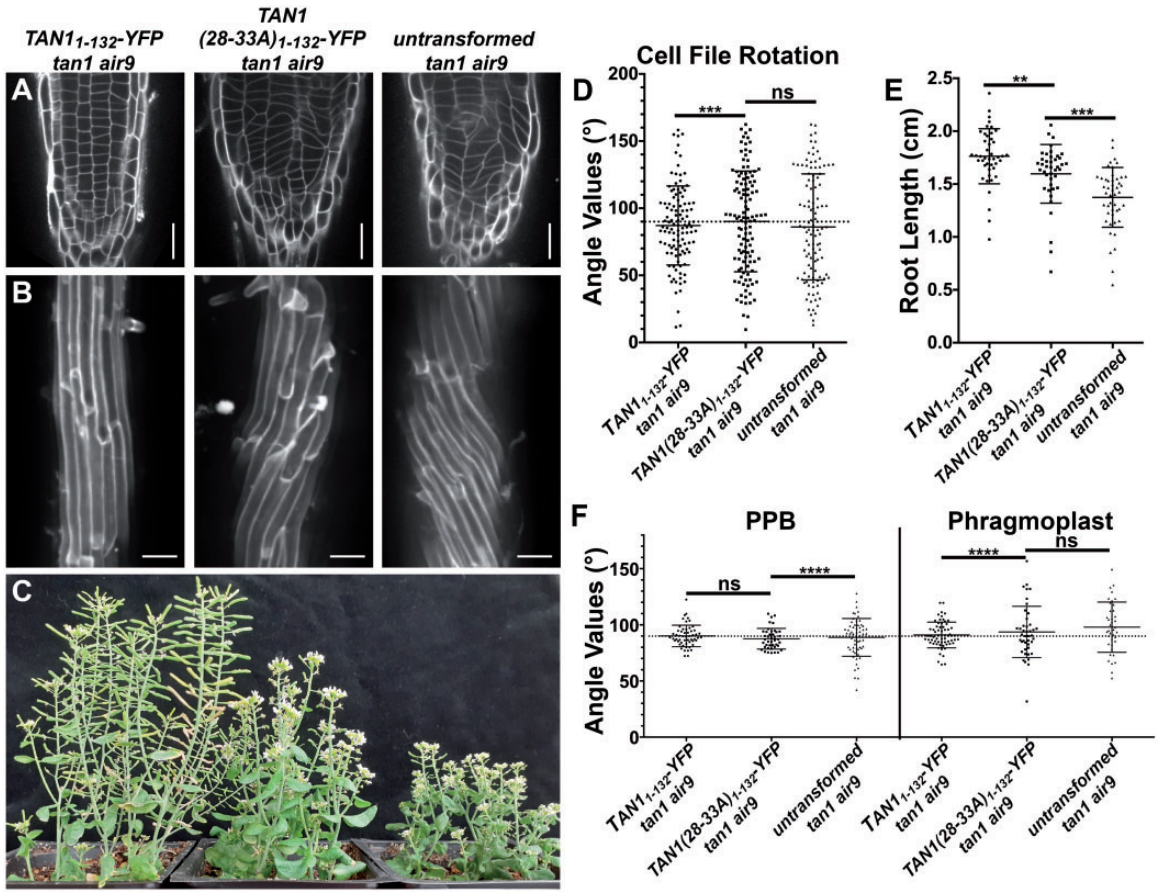

Figure 4 p35S:*TAN1(28–33A)*$_{1–132}$*-YFP* partially rescues *tan1 air9* double mutant phenotypes. A, Cell walls of Arabidopsis *tan1 air9* double mutant root tips stained with PI of plants expressing p35S:*TAN1*$_{1–132}$*-YFP* (left), p35S:*TAN1(28–33A)*$_{1–132}$*-YFP* (middle), and untransformed *tan1 air9* double mutant plants (right). Scale bars = 25 µm. B, Maximum projections of 10 1-µm Z-stacks of PI-stained differentiation zone root cell walls. Scale bars = 50 µm. C, Fifty-eight-day-old *tan1 air9* double mutant plants expressing p35S:*TAN1*$_{1–132}$*-YFP* (left), p35S:*TAN1(28–-33A)*$_{1–132}$*-YFP* (middle), and untransformed *tan1 air9* double mutant plants (right). D, Cell file rotation angles of *tan1 air9* double mutant plants expressing p35S:*TAN1*$_{1–132}$*-YFP* (left), p35S:*TAN1(28–33A)*$_{1–132}$*-YFP* (middle), and untransformed *tan1 air9* double mutant plants (right) $n > 27$ plants for each genotype. Variances were compared with Levene's test. E, Root length measurements from 8 days after stratification of *tan1 air9* double mutant plants expressing p35S:*TAN1*$_{1–132}$*-YFP* (left), p35S:*TAN1(28–33A)*$_{1–132}$*-YFP* (middle), and untransformed *tan1 air9* double mutant plants (right), $n > 40$ plants for each genotype, two-tailed *t* test with Welch's correction. F, PPB and phragmoplast angle measurements in dividing root cells of *tan1 air9* double mutant plants expressing p35S:*TAN1*$_{1–132}$*-YFP* (left), p35S:*TAN1(28–33A)*$_{1–132}$*-YFP* (middle), and untransformed plants (right), $n > 17$ plants for each genotype. Angle variance compared with *F*-test. Mean and standard deviation are indicated. ns indicates not significant, $^{**}P < 0.01$, $^{****}P < 0.0001$.

the PPB in 41% of cells (n = 32/79), which is significantly less frequent when compared to 72% of cells (n = 58/82 cells, 20 plants) with PPBs in the *tan1 air9* mutant containing unaltered CFP–TAN1 and YFP–POK1 (Figure 6, A and I; Fisher's exact test, $P = 0.0001$, similar to Lipka et al. (2014) and Schaefer et al., 2017). Unaltered CFP–TAN1 fully rescued the *tan1 air9* double mutant (Mills and Rasmussen, 2022), and served here as a control. Unaltered CFP–TAN1 and YFP–POK1 localized and were maintained at the division site similar to in the WT during metaphase (Figure 6B, n = 13/13), while CFP–TAN1(28–33A) and YFP–POK1 in the *tan1 air9* mutant were sometimes absent from the division site during metaphase with only 58% of metaphase cells maintaining both proteins at the division site (n = 11/19 cells, Figure 6, F and I). During early telophase, unaltered CFP–TAN1 and YFP–POK1 were always at the division site (n = 14/14, Figure 6C), but CFP–TAN1(28–33A) and YFP–POK1 were maintained at the division site in only 65% of early telophase cells (n = 20/31 cells, Figure 6, G and I). Interestingly, YFP–POK1 accumulated in the phragmoplast midline in 26% of early telophase cells (n = 8/31 cells, Figure 6I) but was not observed in the phragmoplast midline in early telophase cells of plants expressing unaltered CFP–TAN1 (n = 0/14 cells, Figure 6I). During late telophase, when the phragmoplast has contacted the cell cortex in at least one location, CFP–TAN1 and POK1 always localized to the division site (100%, n = 63/63 cells, Figure 6D). Interestingly, although not observed in earlier stages, YFP–POK1 and CFP–TAN1(28–33A) recruitment to the division site increased to 90% of late telophase cells

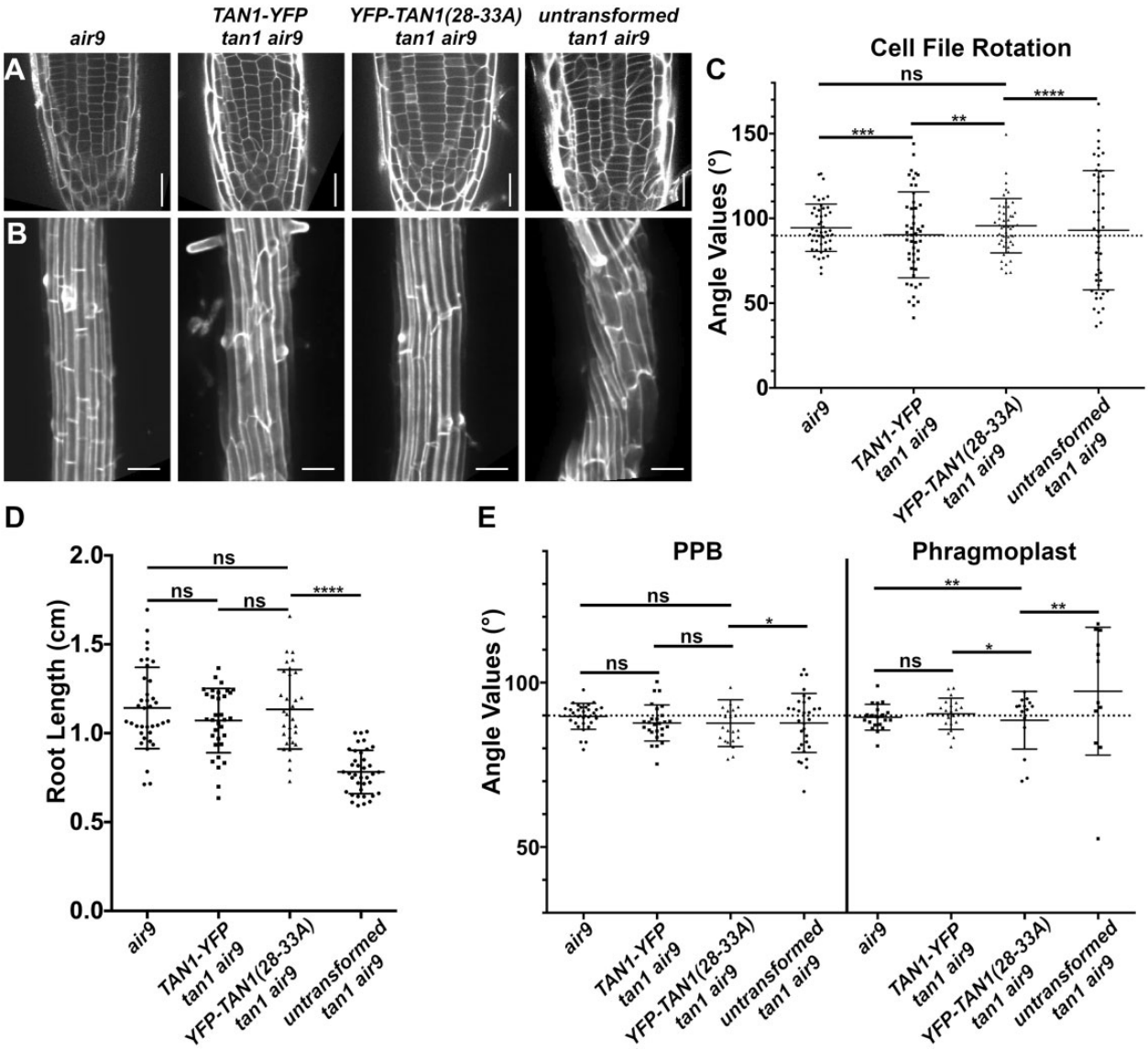

Figure 5 Full-length *TAN1* with alanine substitutions replacing amino acids 28–33 (p35S:*YFP–TAN1(28–33A)*) mostly rescues the *tan1 air9* double mutant. A, PI-stained root tips of an *air9* single mutant plant (left); *tan1 air9* double mutant plants expressing p35S:*TAN1-YFP* (center left) or p35S:*YFP–TAN1(28–33A)* (center right); and an untransformed *tan1 air9* plant (right). Scale bars = 25 μm. B, Maximum projections of 10 1-μm Z-stacks of PI-stained cell walls in the root differentiation zone. Scale bars = 50 μm. C, Cell file rotation angles of *air9* single mutant plants (left); *tan1 air9* double mutant plants expressing p35S:*TAN1-YFP* (center left) or p35S:*YFP–TAN1(28–33A)* (center right); and untransformed *tan1 air9* plants (right), $n > 9$ plants for each genotype. Variances were compared with Levene's test. D, Root length measurements from 8 days after stratification of *air9* single mutant plants (left); *tan1 air9* double mutant plants expressing p35S:*TAN1-YFP* (center left) or p35S:*YFP–TAN1(28–33A)* (center right); and untransformed *tan1 air9* plants (right), $n > 30$ plants of each genotype, compared by two-tailed t test with Welch's correction. E, PPB and phragmoplast angle measurements in dividing root cells of *air9* single mutant plants (left); *tan1 air9* double mutant plants expressing p35S:*TAN1-YFP* (center left) or p35S:*YFP–TAN1(28–33A)* (center right); and untransformed *tan1 air9* plants (right), PPB measurements of $n > 15$ plants for each genotype; phragmoplast measurements of $n > 8$ plants for each genotype. Angle variance compared with *F*-test. ns indicates not significant, $^{*}P < 0.05$, $^{**}P < 0.01$, $^{***}P < 0.001$, $^{****}P < 0.0001$. Mean and standard deviation are indicated.

(n = 53/59 cells, Figure 6H). In the remaining cells, neither CFP–TAN1(28–33) nor YFP–POK1 localized to the division site (3%, n = 2/59), or only CFP–TAN1(28–33) accumulated at the division site (7%, n = 4/59 cells). Together, these data suggest that TAN1–POK1 interactions play a critical role in stabilizing them together at the division site. Additionally, it suggests that other, yet unidentified proteins may recruit both TAN1 and POK1 to the division site, particularly during late telophase, in the absence of both AIR9 and the TAN1–POK1 interaction.

Discussion

In *tan1* and *air9* single mutants, POK1 localizes to the division site and there are no discernable division plane defects (Model in Supplemental Figure S7). However, in the *tan1 air9* double mutant, POK1 co-localizes with the PPB but is

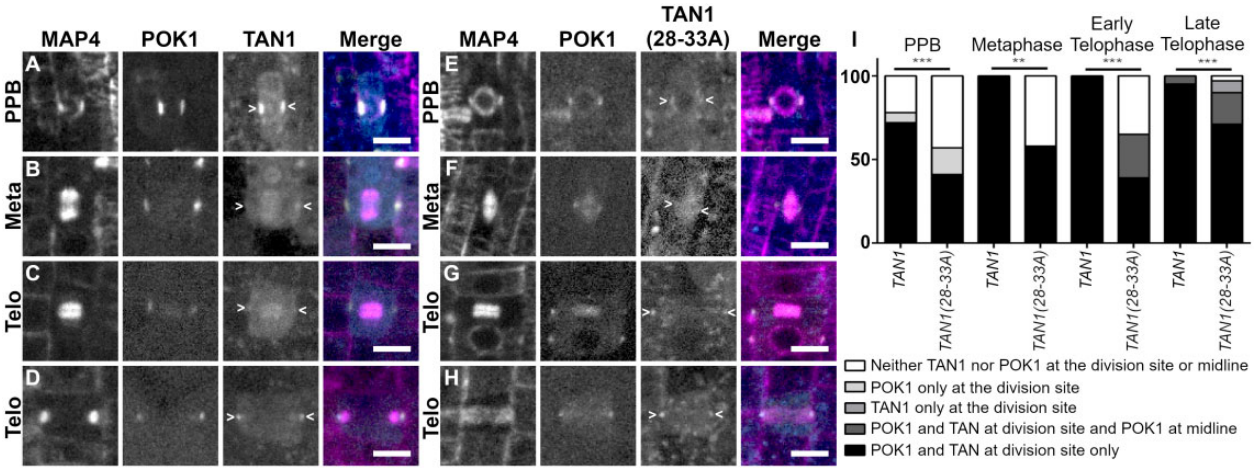

Figure 6 CFP–TAN1(28–33A) and YFP–POK1 exhibit impaired recruitment to the division site in the *tan1 air9* double mutant. YFP–POK1 localization in *tan1 air9* double mutant plants expressing *UBQ10*:mScarlet-*MAP4* and either (A–D) pTAN1:*CFP–TAN1* or (E–I) pTAN1:*CFP–TAN1(28–33A)*. Maximum projections of three 1-μm Z-stacks. Scale bars = 10 μm. Some bleed-through from the mScarlet channel can be seen in the YFP–POK1 panels. A, YFP–POK1 and CFP–TAN1 frequently colocalized with the PPB. B, YFP–POK1 and CFP–TAN1 were maintained at the division site in metaphase. C, YFP–POK1 and CFP–TAN1 were maintained at the division site in all early telophase cells and late telophase. E, YFP–POK1 and CFP–TAN1(28–33A) colocalized with the PPB. F, YFP–POK1 and CFP–TAN1(28–33A) were maintained at the division site in most metaphase cells. CFP–TAN1(28–33A) was faint at the division site. G, Both YFP–POK1 and CFP–TAN1(28–33A) were observed at the division site in most early telophase cells. H, YFP–POK1 and CFP–TAN1(28–33A) were recruited to the division site in late telophase. I, Subcellular localization of CFP–TAN1 and CFP–TAN1(28–33A) in *tan1 air9* double mutant cells during preprophase/prophase, metaphase, early telophase (telophase cells where the phragmoplast has not yet contacted the cell cortex), and late telophase. $N > 19$ plants for each genotype. Statistically significant differences were determined using Fisher's exact test. Asterisks indicate significant differences in POK1 and TAN1/TAN1(28–33A) localization to the division site only. CFP–TAN1 and YFP–POK1 colocalized with the PPB more frequently (72%, 59/82 cells) than CFP–TAN1(28–33A) and YFP–POK1 (41%; 32/79 cells; $P = 0.001$). *tan1 air9* plants expressing *CFP–TAN1(28–33A)* also had more PPBs that only accumulated YFP–POK1 (16%; 13/79 cells; $P = 0.0461$) compared to *CFP–TAN1*-expressing plants (6%, 5/82). In metaphase cells, CFP–TAN1 and YFP–POK1 were maintained at the division site in 100% of observed cells (13/13), compared to CFP–TAN1(28–33A) and YFP–POK1 which accumulated at the division site in 58% of cells (11/19, $P = 0.0104$). In early telophase, TAN1(28–33A) and YFP–POK1 accumulation at the division site was reduced (39%; 12/31 cells, $P = 0.0001$) compared to CFP–TAN1 and YFP–POK1 accumulation (100%, 14/14 cells). *CFP–TAN1(28–33A)*-expressing plants also accumulated both CFP–TAN1(28–33A) and YFP–POK1 at the division site and YFP–POK1 in the phragmoplast midline more frequently in early telophase cells compared to CFP–TAN1 expressing plants (26%; 8/31 cells; $P = 0.0436$). CFP–TAN1(28–33A) and YFP–POK1 were also absent at the division site and phragmoplast midline in a portion of early telophase cells (35%; 11/31 cells; $P = 0.098$). compared to CFP–TAN1 expressing plants (0/14 cells). CFP–TAN1(28–33A) and YFP–POK1 accumulated at the division site in 71% of late telophase cells (42/59 cells) compared to CFP–TAN1 and YFP–POK1 (60/63, $P = 0.0004$) Nineteen percent of late telophase cells accumulated both CFP–TAN1(28–33A) and YFP–POK1 at the division site and YFP–POK1 in the phragmoplast midline (11/59 cells) more frequently compared to CFP–TAN1-expressing plants (3/63 cells; $P = 0.022$). In some late telophase cells of *TAN1(28–33A)*-expressing plants CFP–TAN1(28–33A) accumulated at the division site alone (7%; 4/59 cells; $P = 0.0518$) or TAN1(28–33A) and YFP–POK1 failed to accumulate at the division site (3%; 2/59 cells; $P = 0.2318$) compared to CFP–TAN1-expressing plants where neither localization pattern was observed in late telophase (0/63 cells).

lost from the division site during metaphase (Model in Figure 7). First, this suggests that TAN1 and AIR9 are not essential for POK1 co-localization with the PPB. Second, it suggests that POK1 is maintained at the division site after PPB disassembly via direct or indirect interactions with TAN1 or AIR9. We provide evidence that TAN1 interacts with POK1 through motifs within the first 132 amino acids of TAN1, as identified using the yeast two-hybrid system. Alignments of TAN1 proteins from representative monocots and dicots, such as *Solanum lycopersium*, *Oryza sativa*, *Sorghum bicolor*, *Zea mays*, and *Brassica napus*, showed that amino acids 28–33 (INKVDK) are highly conserved across plant species (Supplemental Figure S8). Amino acids 30–32 (VDK) are identical and the remaining residues within the motif have similar properties across these plant species. The high degree of conservation suggests that these amino acids are likely important for TAN1 function. When alanine substitutions of these amino acids were introduced into TAN1 and transformed into the Arabidopsis *tan1 air9* double mutant, we observed reduced TAN1 and POK1 localization at the division site, as well as defects in phragmoplast positioning. Here, we hypothesize that amino acids 28–33 are essential for TAN1 and POK1 interaction in both the yeast two-hybrid system and in Arabidopsis. In addition to several reports showing that TAN1 and POK1 interact using the yeast two-hybrid system (Müller et al., 2006; Rasmussen et al., 2011), bimolecular fluorescence complementation has also been used to show TAN1–POK1 interactions in Arabidopsis protoplasts (Lipka et al., 2014). Alanine substitutions at positions 28–33 of TAN1 may disrupt TAN1–POK1 interactions through misfolding that blocks the POK1 interaction site or by affecting the amino acids that directly

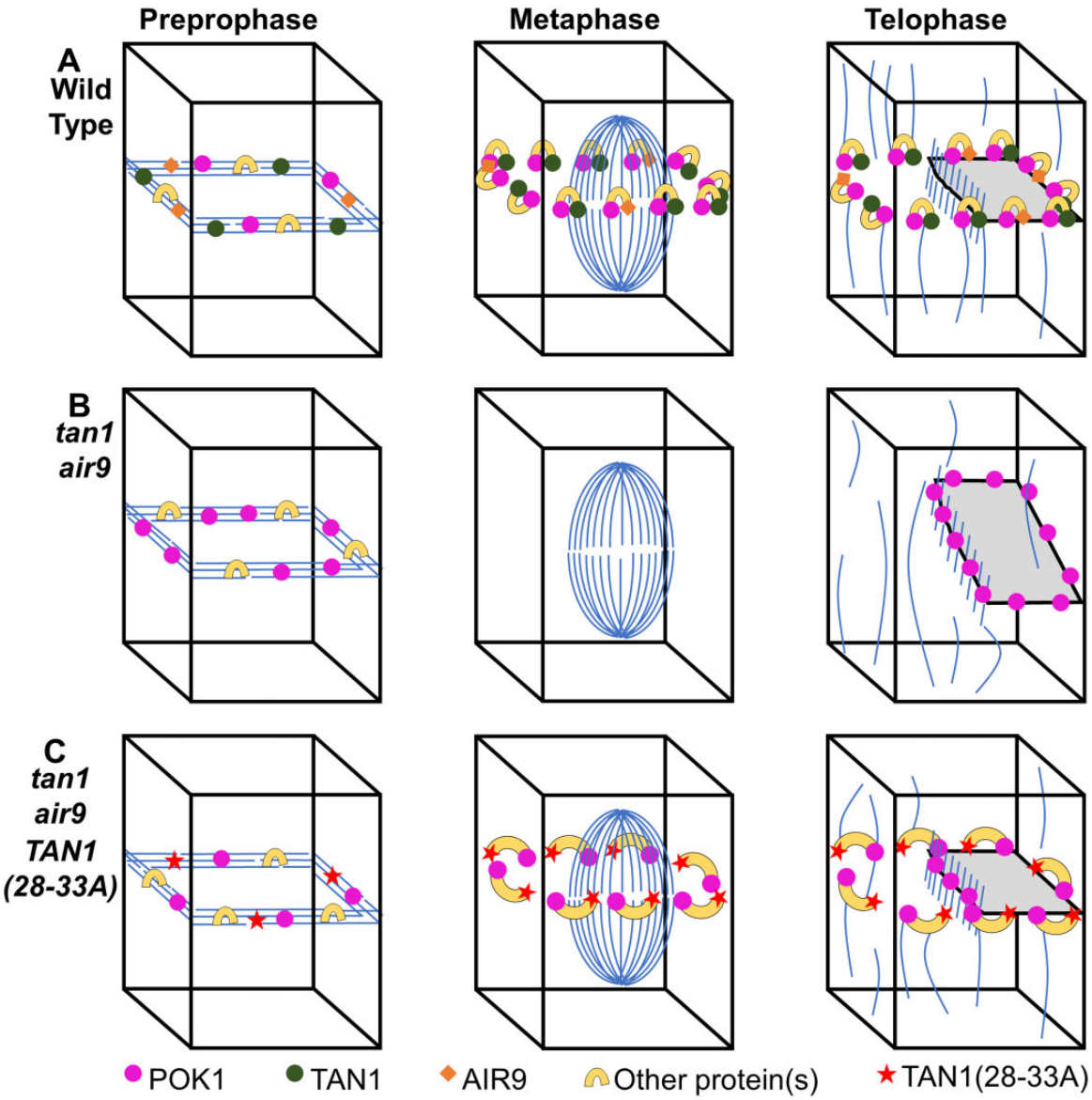

Figure 7 Speculative model of TAN1, AIR9, and POK1 interactions to ensure correct division plane orientation. A, In WT cells, AIR9, TAN1, and POK1 are recruited independently of one another to the PPB. Interaction between TAN1 and POK1 maintains both proteins at the division site through telophase, with AIR9 being re-recruited to the division site in late telophase. B, In the *tan1 air9* double mutant, TAN1, AIR9, and potential AIR9/POK1 interacting proteins are recruited to the PPB. Upon disassembly of the PPB, POK1 is lost from the division site and during telophase aberrantly accumulates in the phragmoplast midline. Due to the loss of TAN1 and POK1 from the division site, the phragmoplast is not guided to the location defined by the PPB. C, In the *tan1 air9* double mutant expressing *TAN1(28–33A)*, TAN1(28–33A), and POK1 are recruited to the PPB independently of one another. POK1 and TAN1(28–33A) are partially maintained in some metaphase and early telophase cells possibly by interactions with other proteins. However, due to the inability of TAN1(28–33A) and POK1 to interact with one another, both proteins are not efficiently maintained at the division site. Most (90%) late telophase cells contain both POK1 and TAN1(28–33A) at the division site. Late recruitment of POK1 and TAN1(28–33A) may help guide the phragmoplast to the correct division site in most cells.

mediate POK1 binding. Regardless of the exact mechanism(s) of POK1–TAN1 physical interactions or the possibility that yeast two-hybrid interactions do not reflect equivalent POK1–TAN1 physical interactions in Arabidopsis, we show that these TAN1 amino acids are involved in mediating TAN1 and POK1 localization to the division site.

We demonstrate that the first region of the TAN1 protein, the first 132 amino acids that primarily accumulate at the division site during telophase (Rasmussen et al., 2011), is both necessary (Mir et al., 2018) and sufficient to largely rescue the *tan1 air9* double mutant (Figure 2). This suggests that $TAN1_{1-132}$ and its recruitment to the division site during telophase is critical for correct division plane orientation in the *tan1 air9* double mutant. Although full length TAN1 localizes to the division site throughout cell division, the ability of $TAN1_{1-132}$ to rescue the *tan1 air9* double mutant suggests that TAN1, and possibly POK1, localization to the PPB and division site during metaphase may not be required

for division site maintenance in Arabidopsis. Indeed, whether the PPB itself is required for division plane positioning has been raised by analysis of a triple mutant in three closely related genes (*TONNEAU RECRUITING MOTIF6* (*TRM6*), *TRM7*, and *TRM8*). The *trm678* mutant, which lacks well defined PPBs, has partially disrupted POK1 recruitment to the division site but only minor defects in division positioning (Schaefer et al., 2017). However, when amino acids critical for TAN1–POK1 interactions in the yeast two-hybrid system are disrupted by transforming *TAN1(28–33A)$_{1–132}$-YFP* into the *tan1 air9* double mutant, root growth and phragmoplast positioning are disrupted. TAN1(28–33A)$_{1–132}$-YFP accumulation at the division site during telophase was reduced compared to unaltered TAN1$_{1–132}$-YFP. This suggests that TAN1–POK1 interaction promotes, but is not strictly necessary, for TAN1 recruitment to the division site during telophase.

Full-length TAN1(28–33A) localizes to the division site throughout cell division and almost fully rescues the *tan1 air9* double mutant. TAN1, AIR9, and POK1 colocalize at the PPB independently of one another, which may promote the formation of protein complexes required for division site maintenance. Colocalizing with the PPB may provide an opportunity for nearby proteins to form stabilizing interactions before PPB disassembly. This suggests that recruitment of TAN1 and POK1 to the division site early in cell division may provide another temporally distinct way to promote correct division plane positioning. Phragmoplast positioning defects in TAN1(28–33A) *tan1 air9* plants may be the result of defects in phragmoplast guidance in cells that lacked TAN1(28–33A) and POK1 at the division site in metaphase or early telophase that were not corrected in late telophase.

The ability of TAN1(28–33A) and POK1 to remain at the division site in some cells after PPB disassembly in the *tan1 air9* double mutant suggests that there are other proteins that interact with TAN1 and/or POK1 that help stabilize them at the division site perhaps via the formation of multiprotein complexes. The pleckstrin homology GAPs, PHGAP1, and PHGAP2 (Stöckle et al., 2016); RANGAP1 (Xu et al., 2008); and IQ67 DOMAIN (IQD)6,7,8 proteins (Kumari et al., 2021) are division site-localized proteins that may stabilize TAN1 and POK1 at the division site via their interaction with POK1. PHGAP1, PHGAP2, and RANGAP1 are dependent on POK1 and POK2 for division site recruitment. Like TAN1, RANGAP1 colocalizes with the PPB and remains at the division site throughout cell division (Xu et al., 2008). PHGAP1 and PHGAP2 are uniformly distributed in the cytoplasm and on the plasma membrane in interphase cells and accumulate at the division site during metaphase. These proteins also have their own distinct roles in division site maintenance (Stöckle et al., 2016). PHGAP2 has a likely role in division site establishment by regulating ROP activity (Hwang et al., 2008). RANGAP1 regulation of local RAN-GTP levels has potential roles in microtubule organization and division site identity (Xu et al., 2008). IQD6, IQD7, and IQD8 interact with POK1 and play a role in PPB formation and POK1 recruitment to the division site. The *iqd678* triple mutant has PPB formation defects and fails to recruit POK1 to the division site in cells lacking PPBs. However, POK1 localization to the division site in the *iqd678* mutant recovers during telophase to WT levels (Kumari et al., 2021). We speculate that this IQD6–8 independent recruitment may depend on TAN1. Unlike the PHGAPs and RANGAP1, IQD8 localization to the division site is not dependent on POK1 and POK2. This suggests that IQD6–8 proteins work upstream of POK1 to establish the division site and are important for POK1 recruitment to the division site early in cell division. Although TAN1–POK1 interactions become critical for TAN1 and POK1 maintenance at the division site in the absence of AIR9, other division site-localized proteins may provide additional stability and help maintain TAN1 and POK1 at the division site.

How AIR9 stabilizes POK1 at the division site in the absence of TAN1 is less clear. There is no information about whether POK1 and AIR9 interact directly with one another. Additionally, AIR9 localization, in contrast to TAN1 localization, is intermittent at the division site. When expressed in tobacco (*Nicotiana tabacum*) Bright Yellow2 cells, AIR9 colocalizes with the PPB but is then lost from the division site until late telophase when the phragmoplast contacts the cortex (Buschmann et al., 2006). In Arabidopsis, AIR9 may localize to the division site during metaphase or telophase, but it is difficult to observe because AIR9 also strongly colocalizes with cortical microtubules, which may obscure AIR9 localization in nearby cells (Buschmann et al., 2015). Rather than directly interacting with POK1, AIR9 may recruit other proteins to the division site during preprophase that help maintain POK1 at the division site in the absence of TAN1. One potential candidate is the kinesin-like calmodulin binding protein, KCBP, which interacts with AIR9 (Buschmann et al., 2015). KCBP is a minus-end-directed kinesin (Song et al., 1997) that localizes to the division site in Arabidopsis and moss (Miki et al., 2014; Buschmann et al., 2015). We speculate that other TAN1, AIR9, and POK1 interacting proteins that have not been identified yet may be key for TAN1–POK1 division site maintenance.

POK1 and POK2 have roles in phragmoplast guidance, but POK2 also has a role in phragmoplast dynamics (Lipka et al., 2014; Herrmann et al., 2018). Although POK1 does not frequently accumulate in the phragmoplast midline in WT cells, POK2 showed striking dual localization to both the phragmoplast midline and the division site. Localization of POK2 to the phragmoplast midline required the N-terminal motor domain, while the C-terminal region was localized to the division site (Herrmann et al., 2018). Our hypothesis is that the "default" location of both POK1 and POK2 is at microtubule plus ends at the phragmoplast midline, based on likely or confirmed plus end-directed motor activity (Chugh et al., 2018). Interactions with division site-localized proteins, such as TAN1 and AIR9, may stabilize or recruit

POK1 and POK2 at the division site away from the phragmoplast midline.

We demonstrate that AIR9 and TAN1 function redundantly to maintain POK1 at the division site to ensure correct cell wall placement. In the absence of AIR9, our data suggest that TAN1–POK1 interaction promotes, but is not required for, the maintenance of both proteins at the division site, and disrupting this interaction partially disrupts their localization to the division site. This also suggests that other TAN1, POK1, and AIR9 interacting proteins are involved with stabilizing TAN1 and POK1 at the division site.

Materials and methods

Growth conditions, genotyping mutants, and root length measurements

Arabidopsis (*A. thaliana*) seedlings were grown on 1/2 strength Murashige and Skoog (MS) media (MP Biomedicals; Murashige and Skoog, 1962) containing 0.5 g L^{-1} morpholineethanesulfonic acid monohydrate (MES-monohydrate, Fisher Scientific, Waltham, MA, USA, CAS 145224-94-8), pH 5.7, and 0.8% agar (Fisher Scientific). Seeds sown on plates were first stratified in the dark at 4°C for 2–5 days, then grown vertically in a growth chamber (Percival) with 16-h white light ~111 $\mu E^{*}m^{-2}s^{-1}$ (F17T8/TL741 Fluorescent Tube (Philips)/8-h dark cycles and the temperature set to 22°C. For root length experiments, *tan1 air9* transgenic T3 lines expressing p35S:*TAN1-YFP*, p35S:*TAN1*$_{1-132}$-*YFP*, p35S:*TAN1(28–33A)*$_{1-132}$-*YFP*, or p35S:*YFP–TAN1(28–33A)* were grown vertically, the plates were scanned (Epson) and root lengths were measured using FIJI (ImageJ, http://fiji.sc/) after 8 days. Untransformed *tan1 air9* double mutant and *air9* single mutant seeds were grown alongside the double mutant seeds expressing the TAN1 constructs in equal numbers on the same plates to ensure plants were grown under the same conditions. After plates were scanned, seedlings were screened by confocal microscopy to identify seedlings expressing YFP translational fusion transgenes and CFP-TUBULIN, if present in the transgenic lines. At least three biological replicates, grown on separate plates on separate days, and at least 28 plants of each genotype across all replicates were analyzed for each root growth experiment. Welch's *t* tests were used to identify whether there were statistically significant differences between replicates before pooling the replicates for analysis. Root lengths were then plotted using Prism (GraphPad). Statistical analysis of root length was performed with Prism (GraphPad) using *t* tests with Welch's correction. Welch's *t* test (unequal variance *t* test) is used to test the hypothesis that two populations have equal means. Unlike the Student's *t* test, Welch's *t* test is often used when two samples have unequal variances or sample sizes. This test was used due to the unequal sample sizes because the plants examined were often segregating for multiple transgenes and had lower sample sizes than control plants such as the *air9* single mutant and *tan1 air9* double mutant, which either lacked transgenes or were segregating fewer transgenes.

YFP translational fusion TAN1 constructs were analyzed in *csh-tan* (*TAN1*, AT3G05330) *air9-31* (*AIR9*, AT2G34680) double mutants in Landsberg *erecta* (*Ler*) unless otherwise specified. The pPOK1:*YFP–POK1* transgene in Columbia, a kind gift from Sabine Müller (Lipka et al., 2014), was crossed into the *tan-mad* and *air9-5* Columbia/Wassilewskija double mutant previously described (Mir et al., 2018). *tan-mad* and *air9-5* mutants were genotyped with primers ATRP and ATLP (to identify WT *TAN1*), JL202 and ATLP (to identify T-DNA insertion in *TAN1*), AIR9-5RP and AIR9-5LP (to identify WT *AIR9*), and LBb1.3 and AIR9RP (to identify T-DNA insertion in *AIR9*) and by observation of the *tan1 air9* double mutant phenotype (Supplemental Table S1).

Generation of transgenic lines

Agrobacterium tumefaciens-mediated floral dip transformation was used as described (Clough and Bent, 1999). *csh-tan air9-31* double mutants were used for all floral dip transformations unless otherwise specified. Transgenic plants were selected on 15 μg mL^{-1} glufosinate (Finale; Bayer) and screened by microscopy before being transferred to soil and selfed. *CFP-TUBULIN* was crossed into p35S:*TAN1(28–33A)*$_{1-132}$-*YFP tan1 air9* plants using *tan1 air9 CFP-TUBULIN* plants (Mir et al., 2018), and progeny were subsequently screened by microscopy for CFP and YFP signal. *csh-tan1 air9-31* double mutants were confirmed by genotyping with primers ATLP and AtTAN 733-CDS Rw (to identify WT *TAN1*), AtTAN 733-CDS Rw and Ds5-4 (to identify T-DNA insertion in *TAN1*), AIR9_cDNA 2230 F and AIR9 gnm7511 R (to identify WT *AIR9*), and AIR9 gnm7511 R and Ds5-4 (to identify T-DNA insertion in *AIR9*).

Columbia expressing the microtubule marker *UBQ10*:mScarlet-*MAP4* (Pan et al., 2020), a kind gift from Xue Pan and Zhenbiao Yang (UCR), was crossed to *tan-mad* and *air9-5* Columbia/Wassilewskija double mutants expressing pPOK1:*YFP–POK1*. Progeny was screened for mScarlet-MAP4 and YFP–POK1 by confocal microscopy and then selfed to recover *air9-5* single mutants, *tan-mad* single mutants, and *air9-5 tan-mad* double mutants expressing mScarlet-*MAP4* and *YFP–POK1*.

pTAN1:*CFP–TAN1* and pTAN1:*CFP–TAN1(28–33A)* were introduced into *air9-5 tan-mad* double mutants expressing mScarlet-*MAP4* and *YFP–POK1* by *A. tumefaciens*-mediated floral dip transformation. pTAN1:*CFP–TAN1* and pTAN1:*CFP–TAN1(28–33A)* transformants were selected on 100 μg mL^{-1} gentamicin (Fisher Scientific) and the presence of mScarlet-MAP4, YFP–POK1, and either CFP–TAN1 or CFP–TAN1(28–33A) was confirmed by confocal microscopy. Four independent T2 transformed lines for pTAN:*CFP–TAN1(28–33A)* and three independent T2 transformed lines for unaltered pTAN:*CFP–TAN1* were examined for division site localization cell counts.

Plasmid construction

TAN1$_{1-132}$-*YFP* coding sequences were subcloned by EcoRI and BamHI double digestion from the plasmid pEZRK-LNY-*TAN1*$_{1-132}$-*YFP* described previously (Rasmussen et al., 2011)

into the pEZT-NL vector (a kind gift from David Ehrhardt, Carnegie Institute, Stanford University) and selected with glufosinate (Finale; Bayer). The CFP-TUBULIN (CFP-TUA6) vector was previously described, a kind gift from Viktor Kirik (Kirik et al., 2007).

Six amino acid alanine substitutions were generated using overlapping polymerase chain reaction (PCR) (primers in Supplemental Table S1) beginning at amino acid 10 of $TAN1_{1-132}$. The $TAN1_{1-132}$-*YFP* coding sequence from plasmids described previously was used as the PCR template (Rasmussen et al., 2011). *TAN1(28–33A)*$_{1-132}$-*YFP* was subcloned by EcoRI–BamHI double digestion into pEZT-NL. To generate *YFP–TAN1(28–33A)*, alanine substitutions were first introduced into G22672 (TAN1 cDNA in pENTR223, from the Arabidopsis Biological Resource Center) using overlapping PCR with the same primers to generate *TAN1(28–33A)*. Gateway LR reaction (Fisher Scientific) was then used to subclone *TAN1(28–33A)* into pEarley104 (Earley et al., 2006).

pTAN:*CFP–TAN1(28–33A)* was generated using overlapping PCR. The TAN1 native promoter was amplified from *Np:AtTAN-YFP* (Walker et al., 2007) using the primers NpTANSacIFor and NpTANceruleanRev. Cerulean was amplified from the Cerulean CDS in pDONR221P4r/P3r using the primers NpTANceruleanFor and CeruleanpEarleyRev. TAN1(28–33A) in pEarley104 was amplified using CeruleanpEarleyFor and pEarleyOCSPstIRev. TAN1 native promoter, Cerulean, and TAN1(28–33A) were then combined using overlapping PCR using NpTANSacI and pEarleyOCSPstIRev. pTAN:*CFP–TAN1(28–33A)* was then subcloned into pJHA212G, a kind gift of Meng Chen (UCR), using SacI and PstI double digest. pTAN:*CFP–TAN1* was generated the same way as pTAN:*CFP–TAN1(28–33A)* except unaltered *TAN1* in pEarley104 was amplified using CeruleanpEarleyFor and pEarleyOCSPstIRev.

Microscopy

An inverted Ti Eclipse (Nikon, Tokyo, Japan) with motorized stage (ASI Piezo) and spinning-disk confocal microscope (Yokogawa W1) built by Solamere Technology was used with Micromanager software (micromanager.org). Solid-state lasers (Obis) and emission filters (Chroma Technology) were used. For CFP translational fusions, an excitation of 445 and emission of 480/40 were used; for YFP translational fusions, an excitation of 514 and emission of 540/30 were used; and for propidium iodide (PI), Alexa-568 goat anti-mouse antibody, and mScarlet-MAP4, an excitation of 561 and emission of 620/60 were used. A 20× objective with a 0.75 numerical aperture and a 60× objective with a 1.2 numerical aperture were used with perfluorocarbon immersion liquid (RIAAA-6788 Cargille). Excitation spectra for mScarlet-MAP4 and YFP–POK1 partially overlapped, which resulted in a faint bleed-through signal in the YFP channel for some dense microtubule structures (e.g. spindles and phragmoplasts). YFP–POK1 colocalization with PPBs was carefully determined based on distinct YFP–POK1 signal and the presence of cytosolic YFP–POK1.

The ratio of the division site versus cytosolic fluorescence intensity was determined by taking the median YFP fluorescence intensity from the center Z-stack of individual cells with PPBs or phragmoplasts. For each cell, the median fluorescence intensity was measured for two cytosolic areas and the division site on each side of the cell using circles with areas of 0.875 μm^2. The sum of the median intensity at the division site on each side was then divided by the sum of the median intensity of the two cytosolic areas to calculate the ratio of the division site versus cytosolic fluorescence intensity. Fluorescence intensities were measured in FIJI. All plants used for this analysis were grown on the same day and imaged using identical conditions, and at least five plants of each genotype were examined.

Measurements of PPB and phragmoplast angles and cell file rotation

At least three biological replicates, grown on separate plates on separate days, composed of at least 15 plants per genotype for PPB measurements and at least eight plants per genotype for phragmoplast measurements were used to gather angle data. Eight-day-old seedlings were stained with 10-μM PI for 1 min and then destained in distilled water before imaging by confocal microscopy using a 20× or 60× objective. PPB and phragmoplast angles were measured using FIJI. The angle was measured between the left-hand cell wall and the orientation of the PPB or phragmoplast in the root tips of *tan1 air9* double mutant plants expressing *CFP-TUBULIN* or immunostained microtubules (described in the next section). Cell file rotation was examined by measuring from the left-hand side of the transverse cell wall relative to the long axis of the root in images of the differentiation zone stained with PI. The differentiation zone was identified by the presence of root hairs. Prism (GraphPad) and Excel (Microsoft Office) were used to perform statistical analyses and to plot data. *F*-tests were used to compare normally distributed variances (PPB and phragmoplast angles) and Levene's tests were used to compare nonnormally distributed variances (cell file rotation angle measurements). The *tan1 air9* double mutant has nonnormally distributed cell file twisting because the roots tend to twist to the left (Mir et al., 2018). Genotypes across biological replicates were compared to ensure there were no statistically significant differences between them before pooling data.

Immunostaining

air9, *tan1 air9* p35S:*TAN1-YFP*, *tan1 air9* p35S:*YFP–TAN1(28–33A)*, and untransformed *tan1 air9* plants were stratified and then grown vertically on 1/2 MS plates in a growth chamber at 22°C with a 16-h/8-h light/dark cycle for 8 days. The seedlings were screened by microscopy for YFP and then fixed and processed for immunofluorescence microscopy using a 1:2,000 dilution of monoclonal anti-α-tubulin B-5-1-2 antibody (Life Technologies, Carlsbad, CA, USA; 32–2500) followed by 1:2000 dilution of Alexa-568 goat anti-mouse antibody (Thermo Fisher, Waltham, MA,

USA; A-11004) as described previously (Sugimoto et al., 2000).

Yeast two-hybrid

Six alanine substitutions were generated using the overlapping PCR and TAN1 coding sequence in pEZRK-LNY-*TAN1*$_{1-132}$*-YFP* as a template beginning at amino acid 10 of TAN1 and continuing through to amino acid 123 according to Russell and Sambrook (2001). All amino acids except substitutions for 64–69 and 106–111 were cloned into the pAS vector (Fan et al., 1997) using EcoRI–BamHI double digestion. pBD-*TAN1(28–33A)* was generated using primers Ala_05_FOR and Ala_05_REV to perform DpnI-mediated site-directed mutagenesis by PCR (Fisher and Pei, 1997). pBD-*TAN1* (Walker et al., 2007) and pAS-*TAN1*$_{1-132}$ (Rasmussen et al., 2011) were used as positive controls, while pAD-MUT was used as a negative control for testing interactions with pAD-*POK1* (Müller et al., 2006). pAD-*POK1* and pAS-*TAN1*$_{1-132}$ constructs were co-transformed into yeast strain YRG2 according to manufacturer instructions (Stragene). A positive yeast two-hybrid interaction was determined by the presence of growth on plates cultured at 30°C lacking histidine after 3 days. Plates were then scanned (Epson, Nagano, Japan).

Accession numbers

TAN1: AT3G05330, AIR9: AT2G34680, and POK1: AT3G17360

Supplemental data

The following materials are available in the online version of this article.

Supplemental Figure S1. *p35S:TAN1*$_{1-132}$*-YFP tan1 air9* lines show significant rescue compared to untransformed *tan1 air9* double mutants

Supplemental Figure S2. Yeast-two-hybrid interactions between POK1 (C-terminal amino acids 1,683–2,066, as previously described; Müller et al., 2006; Rasmussen et al., 2011; Lipka et al., 2014) and TAN1$_{1-132}$ alanine scanning constructs.

Supplemental Figure S3. *p35S:TAN1(28–33A)*$_{1-132}$*-YFP tan1 air9 lines* show variable and incomplete rescue compared to unaltered *p35S:TAN1*$_{1-132}$*-YFP tan1 air9*.

Supplemental Figure S4. Yeast-two-hybrid interactions between TAN1 and POK1 (C-terminal amino acids 1,683–2,066, as previously described'; Müller et al., 2006; Rasmussen et al., 2011; Lipka et al., 2014) and TAN1(28–33A).

Supplemental Figure S5. *p35S:YFP–TAN1(28–33A) tan1 air9* lines show significant rescue compared to untransformed *tan1 air9*, but less accumulation of YFP–TAN1(28–33A) during telophase.

Supplemental Figure S6. YFP–TAN1(28–33A) localizes to the division site in preprophase or prophase and with reduced fluorescence during telophase in *tan1 air9* mutants.

Supplemental Figure S7. A model of POK1 localization in *tan1* and *air9* single mutants.

Supplemental Figure S8. Alignments of amino acids 1–55 of *A. thaliana* TAN1 with TAN1 homologs from other plant species.

Supplemental Table S1. Primers used for cloning and genotyping.

Supplemental Data Set 1. Statistical analysis of tables.

Acknowledgments

Thanks to Andrew Gomez (UCR, supported by USDA-NIFA 2017-38422-27135) for help with yeast two-hybrid experiments, Prof. Sabine Müller (University of Tübingen) for YFP–POK1 seeds, and Profs. Meng Chen and David Nelson (UCR) for their helpful comments on alanine scanning mutagenesis. Thanks to Prof. Henrik Buschmann (Osnabrück University) for original *tan1 air9* characterization. Thanks to Lindy Allsman, Stephanie Martinez, and Aimee Uyehara (UCR) for helpful comments on the manuscript. NSF-CAREER #1942734, NSF-MCB #1716972, and USDA-NIFA-CA-R-BPS-5108-H are gratefully acknowledged for funding.

Funding

This work was funded by National Science Foundation (NSF) NSF-CAREER #1942734, NSF-MCB #1716972, and United States Deparment of Agriculture (USDA) USDA-NIFA-CA-R-BPS-5108-H to CGR.

Conflict of interest statement. None declared.

References

Bellinger MA, Uyehara AN, Martinez P, McCarthy MC, Rasmussen CG (2021) Cell Cortex Microtubules Contribute to Division Plane Positioning During Telophase in Maize. Cold Spring Harbor Laboratory, Cold Spring Harbor, NY

Buschmann H, Chan J, Sanchez-Pulido L, Andrade-Navarro MA, Doonan JH, Lloyd CW (2006) Microtubule-associated AIR9 recognizes the cortical division site at preprophase and cell-plate insertion. Curr Biol **16**: 1938–1943

Buschmann H, Dols J, Kopischke S, Peña EJ, Andrade-Navarro MA, Heinlein M, Szymanski DB, Zachgo S, Doonan JH, Lloyd CW (2015) Arabidopsis KCBP interacts with AIR9 but stays in the cortical division zone throughout mitosis via its MyTH4-FERM domain. J Cell Sci **128**: 2033–2046

Chugh M, Reißner M, Bugiel M, Lipka E, Herrmann A, Roy B, Müller S, Schäffer E (2018) Phragmoplast orienting kinesin 2 is a weak motor switching between processive and diffusive modes. Biophys J **115**: 375–385

Cleary AL, Smith LG (1998) The Tangled1 gene is required for spatial control of cytoskeletal arrays associated with cell division during maize leaf development. Plant Cell **10**: 1875–1888

Clough SJ, Bent AF (1999) Floral dip: a simplified method for Agrobacterium-mediated transformation of *Arabidopsis thaliana*. Plant J **16**: 735–743

Dixit R, Cyr RJ (2002) Spatio-temporal relationship between nuclear-envelope breakdown and preprophase band disappearance in cultured tobacco cells. Protoplasma **219**: 116–121

Earley KW, Haag JR, Pontes O, Opper K, Juehne T, Song K, Pikaard CS (2006) Gateway-compatible vectors for plant functional genomics and proteomics. Plant J **45**: 616–629

Facette MR, Rasmussen CG, Van Norman JM (2018) A plane choice: coordinating timing and orientation of cell division during plant development. Curr Opin Plant Biol **47**: 47–55

Fan HY, Hu Y, Tudor M, Ma H (1997) Specific interactions between the K domains of AG and AGLs, members of the MADS domain family of DNA binding proteins. Plant J **12**: 999–1010

Fisher CL, Pei GK (1997) Modification of a PCR-based site-directed mutagenesis method. Biotechniques **23**: 570–574

Herrmann A, Livanos P, Lipka E, Gadeyne A, Hauser MT, Van Damme D, Müller S (2018) Dual localized kinesin-12 POK2 plays multiple roles during cell division and interacts with MAP65-3. EMBO Rep **19**: e46085

Hoshino H, Yoneda A, Kumagai F, Hasezawa S (2003) Roles of actin-depleted zone and preprophase band in determining the division site of higher-plant cells, a tobacco BY-2 cell line expressing GFP-tubulin. Protoplasma **222**: 157–165

Hwang JU, Vernoud V, Szumlanski A, Nielsen E, Yang Z (2008) A tip-localized RhoGAP controls cell polarity by globally inhibiting Rho GTPase at the cell apex. Curr Biol **18**: 1907–1916

Karahara I, Suda J, Tahara H, Yokota E, Shimmen T, Misaki K, Yonemura S, Staehelin LA, Mineyuki Y (2009) The preprophase band is a localized center of clathrin-mediated endocytosis in late prophase cells of the onion cotyledon epidermis. Plant J **57**: 819–831

Kirik V, Herrmann U, Parupalli C, Sedbrook JC, Ehrhardt DW, Hülskamp M (2007) CLASP localizes in two discrete patterns on cortical microtubules and is required for cell morphogenesis and cell division in Arabidopsis. J Cell Sci **120**: 4416–4425

Kojo KH, Higaki T, Kutsuna N, Yoshida Y, Yasuhara H, Hasezawa S (2013) Roles of cortical actin microfilament patterning in division plane orientation in plants. Plant Cell Physiol **54**: 1491–1503

Kumari P, Dahiya P, Livanos P, Zergiebel L, Kölling M, Poeschl Y, Stamm G, Hermann A, Abel S, Müller S, et al. (2021) IQ67 DOMAIN proteins facilitate preprophase band formation and division-plane orientation. Nat Plants **7**: 739–747

Lee YRJ, Hiwatashi Y, Hotta T, Xie T, Doonan JH, Liu B (2017) The mitotic function of augmin is dependent on its microtubule-associated protein subunit EDE1 in *Arabidopsis thaliana*. Curr Biol **27**: 3891–3897.e4

Lee YRJ, Liu B (2019) Microtubule nucleation for the assembly of acentrosomal microtubule arrays in plant cells. New Phytol **222**: 1705–1718

Lee YRJ, Li Y, Liu B (2007) Two Arabidopsis phragmoplast-associated kinesins play a critical role in cytokinesis during male gametogenesis. Plant Cell **19**: 2595–2605

Lipka E, Gadeyne A, Stöckle D, Zimmermann S, De Jaeger G, Ehrhardt DW, Kirik V, Van Damme D, Müller S (2014) The phragmoplast-orienting kinesin-12 class proteins translate the positional information of the preprophase band to establish the cortical division Zone in *Arabidopsis thaliana*. Plant Cell **26**: 2617–2632

Li S, Sun T, Ren H (2015) The functions of the cytoskeleton and associated proteins during mitosis and cytokinesis in plant cells. Front Plant Sci **6**: 282

Livanos P, Müller S (2019) Division plane establishment and cytokinesis. Annu Rev Plant Biol **70**: 239–267

Martinez P, Dixit R, Balkunde RS, Zhang A, O'Leary SE, Brakke KA, Rasmussen CG (2020) TANGLED1 mediates microtubule interactions that may promote division plane positioning in maize. J Cell Biol **219**: e201907184

Martinez P, Luo A, Sylvester A, Rasmussen CG (2017) Proper division plane orientation and mitotic progression together allow normal growth of maize. Proc Natl Acad Sci USA **114**: 2759–2764

McMichael CM, Bednarek SY (2013) Cytoskeletal and membrane dynamics during higher plant cytokinesis. New Phytol **197**: 1039–1057

Miki T, Naito H, Nishina M, Goshima G (2014) Endogenous localizome identifies 43 mitotic kinesins in a plant cell. Proc Natl Acad Sci USA **111**: E1053–E1061

Mills AM, Rasmussen C (2022) Action at a distance: Defects in division plane positioning in the root meristematic zone affect cell organization in the differentiation zone. bioRxiv: 2021.04.30.442137

Mir R, Morris VH, Buschmann H, Rasmussen CG (2018) Division plane orientation defects revealed by a synthetic double mutant phenotype. Plant Physiol **176**: 418–431

Müller S, Han S, Smith LG (2006) Two kinesins are involved in the spatial control of cytokinesis in *Arabidopsis thaliana*. Curr Biol **16**: 888–894

Müller S, Jürgens G (2016) Plant cytokinesis—No ring, no constriction but centrifugal construction of the partitioning membrane. Semin Cell Dev Biol **53**: 10–18

Murashige T, Skoog F (1962) A revised medium for rapid growth and bio agsays with tohaoco tissue cultures. Plant Physiol **15**: 473–479

Murata T, Sano T, Sasabe M, Nonaka S, Higashiyama T, Hasezawa S, Machida Y, Hasebe M (2013) Mechanism of microtubule array expansion in the cytokinetic phragmoplast. Nat Commun **4**: 1967

Nakaoka Y, Miki T, Fujioka R, Uehara R, Tomioka A, Obuse C, Kubo M, Hiwatashi Y, Goshima G (2012) An inducible RNA interference system in Physcomitrella patens reveals a dominant role of augmin in phragmoplast microtubule generation. Plant Cell **24**: 1478–1493

van Oostende-Triplet C, Guillet D, Triplet T, Pandzic E, Wiseman PW, Geitmann A (2017) Vesicle dynamics during plant cell cytokinesis reveals distinct developmental phases. Plant Physiol **174**: 1544–1558

Pan R, Lee YRJ, Liu B (2004) Localization of two homologous Arabidopsis kinesin-related proteins in the phragmoplast. Planta **220**: 156–164

Panteris E (2008) Cortical actin filaments at the division site of mitotic plant cells: a reconsideration of the "actin-depleted zone." New Phytol **179**: 334–341

Pan X, Fang L, Liu J, Senay-Aras B, Lin W, Zheng S, Zhang T, Guo J, Manor U, Van Norman J, et al. (2020) Auxin-induced signaling protein nanoclustering contributes to cell polarity formation. Nat Commun **11**: 3914

Rasmussen CG, Bellinger M (2018) An overview of plant division-plane orientation. New Phytol **219**: 505–512

Rasmussen CG, Sun B, Smith LG (2011) Tangled localization at the cortical division site of plant cells occurs by several mechanisms. J Cell Sci **124**: 270–279

Russell DW, Sambrook J (2001) Molecular Cloning: A Laboratory Manual Third. Cold Spring Harbor Laboratory, Cold Spring Harbor, NY

Schaefer E, Belcram K, Uyttewaal M, Duroc Y, Goussot M, Pastuglia M, Bouchez D (2017) The preprophase band of microtubules controls the robustness of division orientation in plants. Science **189**: 186–189

Smertenko, A, Assaad F, Baluška F, Bezanilla M, Buschmann H, Drakakaki G, Hauser MT, Janson M, Mineyuki Y, Moore I, et al. (2017) Plant cytokinesis: terminology for structures and processes. Trends Cell Biol **27**: 885–894

Smertenko A, Hewitt SL, Jacques CN, Kacprzyk R, Liu Y, Marcec MJ, Moyo L, Ogden A, Oung HM, Schmidt S, et al. (2018) Phragmoplast microtubule dynamics - a game of zones. J Cell Sci **131**: jcs203331

Song H, Golovkin M, Reddy AS, Endow SA (1997) In vitro motility of AtKCBP, a calmodulin-binding kinesin protein of Arabidopsis. Proc Natl Acad Sci USA **94**: 322–327

Stöckle D, Herrmann A, Lipka E, Lauster T, Gavidia R, Zimmermann S, Müller S (2016) Putative RopGAPs impact division plane selection and interact with kinesin-12 POK1. Nat Plants **2**: 16120

Suetsugu N, Yamada N, Kagawa T, Yonekura H, Uyeda TQP, Kadota A, Wada M (2010) Two kinesin-like proteins mediate actin-based chloroplast movement in *Arabidopsis thaliana*. Proc Natl Acad Sci USA **107**: 8860–8865

Sugimoto K, Williamson RE, Wasteneys GO (2000) New techniques enable comparative analysis of microtubule orientation, wall texture, and growth rate in intact roots of Arabidopsis. Plant Physiol **124**: 1493–1506

Van Damme D (2009) Division plane determination during plant somatic cytokinesis. Curr Opin Plant Biol **12**: 745–751

Vanstraelen M, Torres Acosta JA, De Veylder L, Inzé D, Geelen D (2004) A plant-specific subclass of C-terminal kinesins contains a conserved a-type cyclin-dependent kinase site implicated in folding and dimerization. Plant Physiol **135**: 1417–1429

Walker KL, Müller S, Moss D, Ehrhardt DW, Smith LG (2007) Arabidopsis TANGLED identifies the division plane throughout mitosis and cytokinesis. Curr Biol **17**: 1827–1836

Wu SZ, Yamada M, Mallett DR, Bezanilla M (2018) Cytoskeletal discoveries in the plant lineage using the moss Physcomitrella patens. Biophys Rev **10**: 1683–1693

Xu XM, Zhao Q, Rodrigo-Peiris T, Brkljacic J, He CS, Müller S, Meier I (2008) RanGAP1 is a continuous marker of the Arabidopsis cell division plane. Proc Natl Acad Sci USA **105**: 18637–18642